CrystEngComm

Cite this: *CrystEngComm*, 2012, **14**, 544

www.rsc.org/crystengcomm

PAPER

Growth mechanism of nanoparticles: theoretical calculations and experimental results

Marcelo M. Mariscal,*[a] J. Jesús Velázquez-Salazar[b] and Miguel Jose Yacaman*[b]

Received 20th May 2011, Accepted 2nd October 2011
DOI: 10.1039/c1ce05602f

We report a combined theoretical and experimental study on the growth mechanism of silver and gold nanoparticles. We introduce for the first time the grand-canonical Monte Carlo method to study the growth/dissolution steps of nanoparticle growth mediated by seeds. In particular we found that small changes on the chemical potential, *i.e.* the activity of the metal ions, produce significant changes on the size and morphologies of the nanoparticles. We have found very good agreements between simulated structures with those observed experimentally by means of scanning electron microscopy.

Introduction

The understanding of the growth mechanism of metallic nanoparticles is very important for technological application, indeed growth control might result in shape control, which is necessary to obtain reproducible results.

A nanocrystal will have in general a polyhedral shape in which the facets correspond to low index planes.[1] Every facet has a different atomic distribution and therefore singular properties.[2] In a typical chemical synthesis firstly a solution of a metallic salt is reduced by the addition of a reducing agent. Subsequently, the atoms start to nucleate until a critical nuclei size is reached. The growth stage then proceeds by the addition of atoms on the growing crystal. In most standard conditions of growth, the polyhedral formed will have internal strain. This is particularly more pronounced on the non-FCC shapes. In fact some non-FCC shapes such as the commonly observed icosahedra particle[3] will have a larger amount of strain, this makes the situation very complex and often it is very difficult to distinguish if the resulting shape results from kinetics or equilibrium, most likely the pure situation does not exist and an intricate correlation between the two possibilities is produced, one in which the nanocrystal has reached a certain size and monoatomic steps can be created on the growing surfaces. If the nanoparticle has developed vicinal surfaces then the steps will persist and will strongly contribute to the growth process.[4]

Therefore, it is of crucial importance to get a better fundamental understanding of shape control for metal nanoparticles. To meet this need, it is of particular interest to investigate the growth mechanisms of metal nanoparticles.

[a]*INFIQC/CONICET, Departamento de Matemática y Física, Facultad de Ciencias Químicas, Universidad Nacional de Córdoba, XUA5000 Córdoba, Argentina. E-mail: marcelo.mariscal@conicet.gov.ar*
[b]*University of Texas at San Antonio, Department of Physics and Astronomy, One UTSA circle, 78249 San Antonio, TX, USA. E-mail: miguel.yacaman@utsa.edu; Tel: +1 210-458-6954*

In the present paper we have performed computer simulations of the growth of Ag and Au nanoparticles using the Monte-Carlo method in the grand canonical ensemble. This technique seems particularly adequate given the complexity of the growth mechanism; we have also made synthesis of relatively large nanoparticles to compare the obtained shapes with the theoretical findings.

Experimental

Synthesis of silver nanostructures

In a typical synthesis,[5] 5 ml of ethylene glycol (EG, 99%) was heated at 160 °C in a flask (equipped with a reflux condenser). Two solutions were prepared, one of the solutions containing 94 mM of silver nitrate ($AgNO_3$, 99.99%) dissolved in 3 ml of EG, and the other one containing 144 mM of poly(vinyl pyrrolidone) (PVP, M_w = 55 000), with 40 μl iron(II) chloride tetrahydrate ($FeCl_2 \cdot 4H_2O$, 99%, 0.04 mM) dissolved in 6 ml of EG. Both solutions were injected (3 ml and 6 ml, respectively) into the hot EG. The reaction was carried out for around 30 min until the solution reaches an ocher color. The samples were washed three times with acetone and once with alcohol to remove excess EG and PVP. During the washing process, the solution was centrifuged for 2 min at 2000 rpm several times. After being purified, the samples were dispersed in alcohol.

Synthesis of gold nanostructures

For the synthesis of gold nanoparticles with slight modifications,[6] 5 ml EG was stirred with a magnetic bar and heated at 250 °C for 10 min. Two solutions were prepared separately, the first solution containing 0.208 g of PVP dissolved in 5 ml EG, and the other 0.08 g of tetrachloroaurate trihydrate ($HAuCl_4 \cdot 3H_2O$, 99.9%) dissolved in 5 ml EG. Then, both solutions were injected simultaneously drop by drop into hot solution. The reaction was carried out for around 10 min until the solution was orange-purple indicating formation of gold nanoparticles. The

products were collected by centrifugation at 4000 rpm for 4 min and were then washed with ethanol several times.

The Ag and Au samples were characterized by an ultra-high resolution scanning electron microscope (STEM) FEG Hitachi S-5500 (0.4 nm at 30 kV) with a BF/DF Duo-STEM detector. Samples for STEM studies were prepared by placing directly the solution onto a holey carbon TEM grid.

Theoretical calculations

To attempt to understand the possible growth/dissolution mechanisms that promote the nanoparticle morphology observed experimentally, we have performed computer simulations using the Monte Carlo method in the grand canonical ensemble.

It is well known that the most frequent growth mechanism of metal nanoparticles in colloidal suspension is the growth of precursor nuclei under given oversaturation conditions. Metal deposition from solution is usually carried out by adding a reducing agent R^u to a solution containing the metal ions (*i.e.* inorganic salt) to be deposited. R^u oxidizes itself to yield the species O^{u+n} and the metal ions reduce to give the metallic species according to the following reaction for Ag NPs:

$$m\mathrm{Ag}^+ + \frac{m}{n}\mathrm{R}^u \rightarrow \frac{m}{n}\mathrm{O}^{u+n} + m\mathrm{Ag}_{\mathrm{cluster}} \quad (1)$$

where u represents the charge of the reduced species and n denotes the number of electrons transferred in the reaction. The corresponding Gibbs free energy change is given by:

$$\Delta G_{n,\mathrm{Agcluster}} = -nF\eta + \Phi(n) \quad (2)$$

where $\Phi(n) = n(\mu_{\mathrm{cluster}} - \mu_{\mathrm{bulk}})$ represents an excess of free energy, required to generate a silver cluster of n atoms at chemical potential μ. The first term in eqn (2) represents the *overpotential* with respect to the bulk deposition of Ag,[7–9] where F is the Faraday constant and η has the meaning of an overpotential that the reducing agent generates with respect to the bulk deposition potential of the metal Ag at the ion activity a^+_{Ag}, the same equations could be written for Au NPs.

The standard ensemble to simulate crystal growth/dissolution is the grand canonical one, where the parameters fixed during the simulation are the volume of the simulation box (V), the temperature (T), and the chemical potential μ of the atoms being deposited (Ag). Thus, we have performed extensive grand canonical Monte Carlo (gcMC) simulations to study the growth/dissolution processes of Ag nanoparticles using realistic semi-empirical interatomic potentials.

The interaction between Ag or Au atoms was calculated according to the embedded atom method (EAM),[10] which is well established that reproduces the main characteristics of the metallic bond, due to the many-body character of the functional form. The Metropolis Monte Carlo (MMC) algorithm[11] was used to sample the configuration space. The importance of the sample scheme in our gcMC procedure involves the following trial moves.

Atomic vibration

This is attempted within a small region, around the coordinate of the i-atom, and the new configuration is accepted with the probability:

$$W_{j\rightarrow i} = \min\left(1, e^{-(\Delta E_{ij}/k_{\mathrm{B}}T)}\right) \quad (3)$$

where ΔE_{ij} is the potential energy change associated with the motion of an atom calculated with the EAM method. This trial move mimics the lattice vibration as well as self-diffusion processes.

Insertion of an atom

An attempt is made to insert a Ag atom at a random position on the surface of the cluster. The new configuration is accepted with a probability:

$$W_{n\rightarrow n+1} = \min\left(1, \frac{V_{\mathrm{acc}}}{\Lambda^3(n+1)} e^{\left(\mu - \Delta E_{n+1,n}/k_{\mathrm{B}}T\right)}\right) \quad (4)$$

where V_{acc} is a volume where the particles are created, Λ is the De Broglie wavelength and $\Delta E_{n+1,n}$ the internal potential energy change due to the creation of an atom on the system.

Removal of an atom

A particle is chosen at random and a removal attempt is accepted with probability:

$$W_{n\rightarrow n-1} = \min\left(1, \frac{\Lambda^3 n}{V_{\mathrm{acc}}} e^{\left(-\mu - \Delta E_{n-1,n}/k_{\mathrm{B}}T\right)}\right) \quad (5)$$

where $\Delta E_{n-1,n}$ the internal potential energy change due to the elimination of an atom on the system. This trial move mimics the dissolution process.

In order to get a good efficiency for the grand canonical MC algorithm, V_{acc} was not the whole volume of the system but a restricted portion of it, located in the neighborhood of the dissolving cluster. Therefore, V_{acc} is the accessible volume to create/delete particles, which is defined as $V_{\mathrm{acc}} = n_s 4/3\pi r_s^3$: where n_s represents the total number of spheres of radius r_s where atoms can be added/deleted in order to satisfy detailed balance.

At this point, it is important to keep in mind that the chemical potential of the metallic species could be defined as:

$$\mu_{\mathrm{M}} = \mu^0_{\mathrm{M}} + RT\ln a_{\mathrm{M}} \quad (6)$$

where a_{M} represents the activity, directly related with the concentration of the metallic salt used, a highly controllable experimental parameter.

Computer simulations results

Ag nanoparticles

Before entering into the gcMC simulations, it is important to define the chemical potential regions where the gcMC calculations will be performed. To do this, the energy contributions from different coordination sites were calculated using the EAM method. Fig. 1 shows the calculated energies for two Ag nanoparticles frequently observed in the experiments shown below, *i.e.* a regular decahedron and a triangular pyramid. The coordination number ξ of each atom is also computed and represented in the figure by means of different colours (see insets of Fig. 1). As expected, surface atoms with lower coordination number have the lower energy. For instance the apex atoms of both,

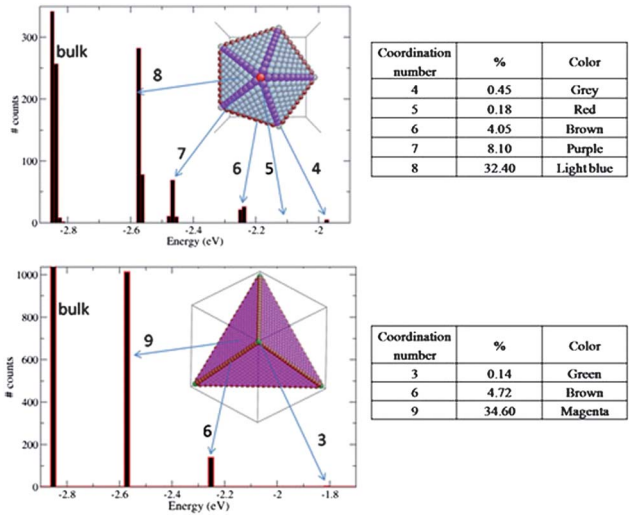

Coordination number	%	Color
4	0.45	Grey
5	0.18	Red
6	4.05	Brown
7	8.10	Purple
8	32.40	Light blue

Coordination number	%	Color
3	0.14	Green
6	4.72	Brown
9	34.60	Magenta

Fig. 1 Energy distribution for different coordination sites. (Upper) Ag regular decahedron and (lower) triangular pyramid. The numbers aside the arrows indicate the coordination number of each site.

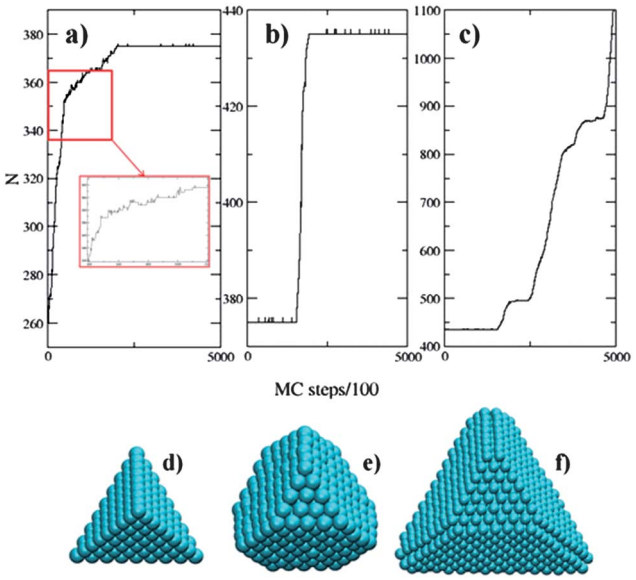

Fig. 2 Upper: number of atoms added to the initial Ag seed as a function of Monte Carlo steps for three chemical potentials ($a = -2.65$ eV, $b = -2.624$ eV, and $c = -2.612$ eV). Lower panel: (d) atomic structure of the initial Ag seed, (e and f) final structure after 5×10^5 MC steps at $\mu = -2.624$ eV and -2.612 eV, respectively.

decahedron and triangular pyramid, show the lower energies: -1.98 and -1.81 eV, respectively. Therefore, it is expected that these sites will be highly unstable with respect to atoms located at closed surfaces. In the case of the regular decahedron, two different border sites can be observed between two {111} surfaces (see the inset of Fig. 1, brown and purple spheres) with energies: -2.25 and -2.48 eV, respectively.

A series of gcMC simulations have been performed, starting from perfect regular decahedron—with 1111 atoms—and triangular pyramid—with 259 atoms—silver seeds as guest clusters. In each simulation 1×10^5 MC steps have been done in order to reach the equilibrium structure at 300 K. The number of MC steps needed was selected in the way that the number of particles on the system reaches a steady state.

Fig. 2 shows the number of Ag atoms as a function of the number of MC steps for a silver triangular pyramid seed (see Fig. 2d). Several steps are observed in the curve (see the inset of curve a), indicating that some structures are particularly stable. It is interesting to note also that the deposition/dissolution processes are evident in the inset of Fig. 2a (several jumps/fluctuations in N). In order to visualize the structure at different stages, several snapshots of the atomic configurations are shown in Fig. 2d–f. It is interesting to note that structures (e) and (f) resemble those observed experimentally, even at considerable smaller size. As expected from the energetic analysis performed above, low-coordination sites are less stable than {111} closed-facets sites, therefore structures exposing {111} surfaces will be energetically more stable. As observed in Fig. 2, the chemical potential of the Ag species plays a key role in the morphology and size of the nanoparticles. For instance, a small change of chemical potential, $\Delta\mu = 0.038$ eV, produces a strong transformation in morphology and size (from ~375 to 1100 atoms).

Although, the Monte Carlo steps are not directly related to the real time, nevertheless, our grand canonical simulations give at least a qualitative idea on the kinetics of cluster growth or dissolution, particularly about the sequence in which atoms are removed or added from energetic considerations. In this sense our simulations predict that silver nanoparticles will grow (starting with a triangular pyramid seed) to truncated pyramid with an absence of border atoms between adjacent *fcc* (111) facets, in good agreement with some of the structures observed experimentally (see below).

We have also considered triangular Ag plates composed of 98 atoms with stacking faults as initial seeds, due to the fact that they are frequently observed in the early stages of the synthesis of silver nanoparticles. In Fig. 3 the number of silver atoms as a function of MC steps is shown. Several atomic structures taken from the simulations are also plotted. Surprisingly, the initial Ag plate evolves towards a decahedron with some truncated apex, which remains stable for several MC steps, indicated by the plateau in the N *vs.* MC step curve. The final structure, as well the

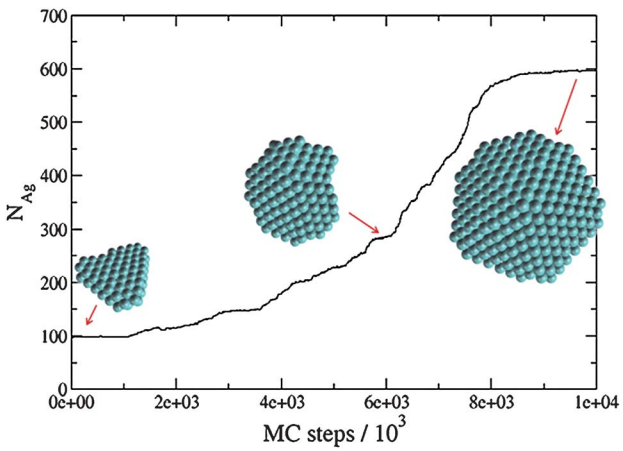

Fig. 3 Number of Ag atoms added to the initial triangular Ag plate (98 atoms) as a function of Monte Carlo steps for $\mu = -2.65$ eV. Inset: selected atomic configurations.

intermediate one, where an incomplete decahedron is formed, resembles very well the structure observed experimentally (shown below).

We have also considered small regular-decahedron seeds to perform grand canonical Monte Carlo calculations. In order to illustrate the dissolution regime, in Fig. 4 the number of Ag atoms as a function of Monte Carlo steps for two chemical potentials is plotted. For example, at −2.39 eV only low-coordinated sites are dissolved, *i.e.* atoms with coordination number smaller than 6 (see Fig. 1). However, tuning a little bit the chemical potential of the silver atoms, *i.e.* changing the activity or the concentration of ions, dissolution from corners and apex will follow. Some selected configurations are also plotted in the inset of Fig. 4. For the last structure, a surface mesh has been created in order to try to compare the simulated structures with those observed experimentally with SEM. From this figure, it is interesting to observe the holes formed on the apex of the regular decahedron and the channels forming {100} surfaces.

This kind of simulation tries to realistically emulate the dissolution process under the digestion mechanism, where a particle is dissolved—not completely—and at the same time another one grows.

Au nanoparticles

The same kind of grand canonical MC simulations were performed for Au seeds of several initial morphologies, *i.e. fcc* truncated octahedra, icosahedra, triangular plates and regular decahedra.

In Fig. 5 the number of gold atoms as a function of the number of MC steps for two chemical potentials is plotted. In this case a *fcc* seed with truncated octahedral shape was used as initial structure. As can be observed in the atomic configurations shown in the inset of Fig. 5, the growth mechanism proceeds through facets, converting all {100} open faces on more closed surfaces, *i.e.* {111}, leading finally to a closed-shell octahedral with stacking faults.

The same triangular plate used for silver—composed of 98 atoms with stacking faults—was used to study the growth of Au nanocrystals. In Fig. 6 the number of Au atoms *vs.* MC steps is

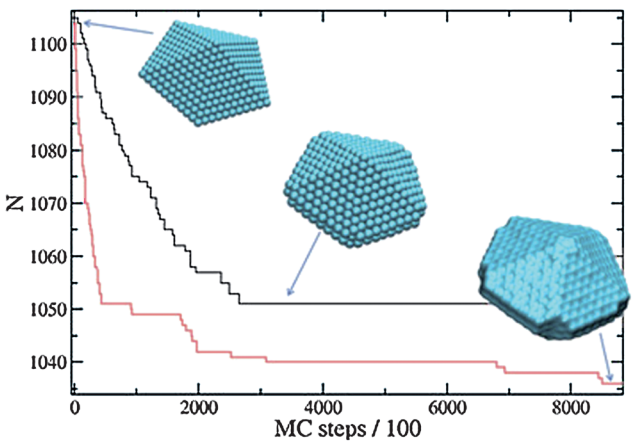

Fig. 4 Number of Ag atoms as a function of Monte Carlo steps for two chemical potentials: −2.39 eV (black line) and −2.44 eV (red line).

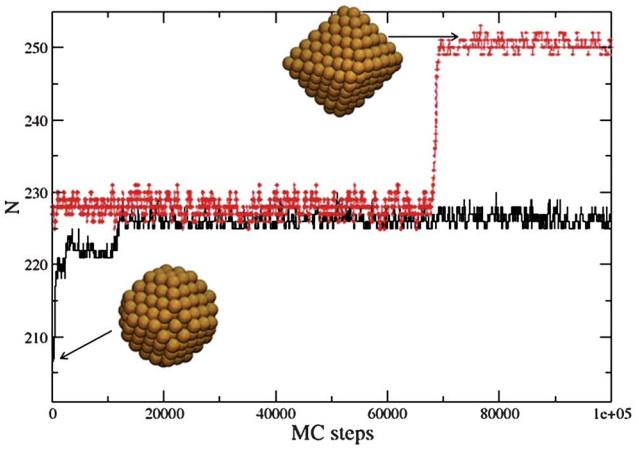

Fig. 5 Number of Au atoms as a function of MC steps for two chemical potentials: −3.70 eV (black line) and −2.65 eV (red).

shown for two relevant chemical potentials. Several meta-stable states are identified by plotting the normalized energy per atom as a function of *N* (see arrows in the right-panel of Fig. 6).

It is interesting to note the particle with *ca.* 430 atoms which is trapped in a local minimum (see Fig. 6, right) and which resembles an incomplete decahedral nanoparticle.

We have also considered icosahedron Au seeds to perform grand canonical Monte Carlo calculations. In order to explore the dissolution regime, in Fig. 7 the number of Au atoms as a function of Monte Carlo steps for three chemical potentials is plotted. For example, at −4.00 eV only low-coordinated sites are dissolved, *i.e.* atoms at the vertices of the icosahedra. However, modifying slightly the chemical potential of Au atoms, dissolution from lines and facets will follow. Some selected configurations are also plotted in the inset of Fig. 7. A surface mesh has been created in order to try to compare the simulated structures with those observed experimentally with SEM in Fig. 11. It is interesting to observe the holes formed on the apex of the icosahedra which are also observed experimentally, indicating that some particular meta-stable states were trapped. Another relevant result observed with the gcMC simulations is that the

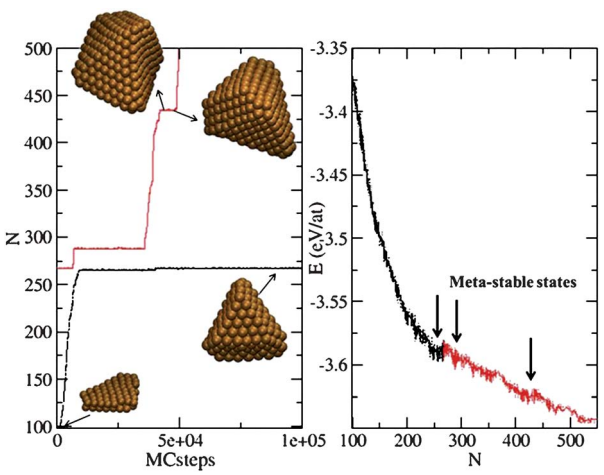

Fig. 6 (Left) Number of Au atoms *vs.* MC steps for two chemical potentials (black: −3.60 eV and red −3.58 eV). (Right) Energy per atom, as a function of the number of Au atoms.

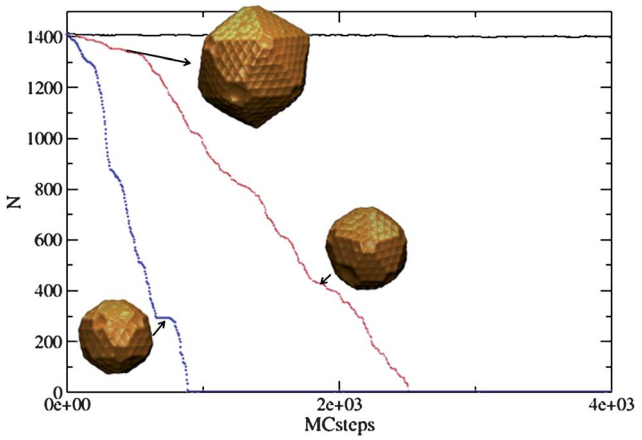

Fig. 7 Number of Au atoms as a function of Monte Carlo steps for three chemical potentials: −4.00 eV (black line), −4.10 eV (red line) and −4.15 eV (blue line).

icosahedra structure dissolves through the shells, keeping the initial morphology (see for example the nanocrystal with *ca.* 400 atoms).

Experimental results

Nanoparticles of gold and silver were synthesized by the polyol method. The Ag nanoparticles were prepared by reducing the $AgNO_3$–$FeCl_2$–PVP–EG solution. When using a low concentration of $FeCl_2$, nanoparticles obtained were triangular, bi-pyramids, tetrahedra and decahedra with truncated corners and edges. On the other hand when using a high concentration of $FeCl_2$ solution, the Ag nanowire was obtained. This occurred because the single crystalline structures were obtained due to the interaction between Fe(II) and Cl^-, which removes the oxygen from the surface of seeds leaving only the single-crystal particles to grow. The low concentration of $FeCl_2$ reduces the oxygen partially from the surface resulting in truncated corners and edges.[5]

When Au nanoparticles were prepared from a $HAuCl_4 \cdot 3H_2O$–PVP–EG solution, the outcome was similar to the silver, yielding similar structures such as: tetrahedral, triangular, bi-pyramidal and decahedral, with truncated corners and edges. This occurred because the Cl^- ions can take part in the oxidative etching of gold nanostructures at high temperatures where the reduction of Au^{3+} to Au^0 in EG occurs.[12]

Nanoparticles of gold and silver grown by the methods above described have shapes which agree with our calculations. We show some examples in Fig. 8 for *fcc* structures and in Fig. 9 for decahedral particles. It is possible to observe that the faceting is produced as a function of the growing particle, and verified by our calculations. Particles develop wedges and extra facets that increase the stability. In most cases the particle will start with (111) facets, then develop extra (100) facets and in few cases (110) faces (shown in Fig. 9b and c).

However the addition of extra faces allows the particle to grow keeping the overall shape. Extreme cases of facing are shown in Fig. 10 for decahedral structures. In this case, heavy truncation can be produced on the center and on the edges as shown in

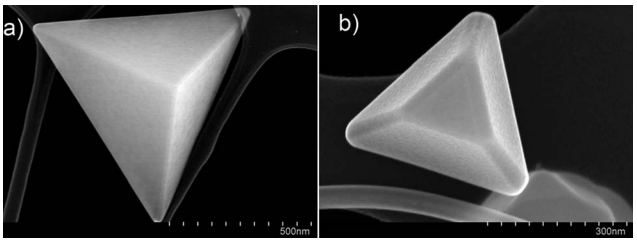

Fig. 8 Examples of Ag nanoparticles based on the tetrahedron shape: (a) non-truncated shape and (b) truncated shape.

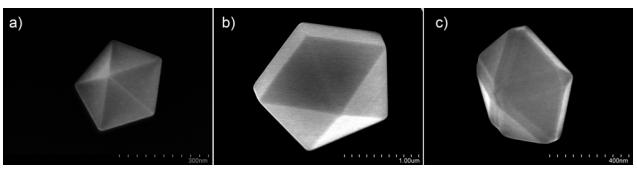

Fig. 9 Decahedral particles: (a) regular Ag decahedron, (b) the gold decahedron has a small growth along [100] directions and the (110) faces are bound by the (111) surface, and (c) truncated Ag decahedron in the corners and along the twin boundaries.

Fig. 10. There are many ridges and wedges in the facets. This kind of faceting was proposed initially by Marks[13] for the decahedral shape.

Icosahedra structures are very interesting and have been the subject of many papers.[14–16] In this case the function is also

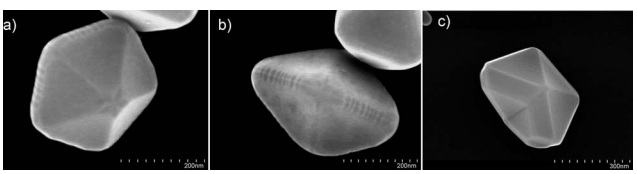

Fig. 10 Examples of heavily truncated decahedra: (a) Au structure truncated on the center of the five-fold axis, (b) top view of a Au decahedron showing parallel oriented defects which are extra steps, and (c) Ag incomplete decahedra.

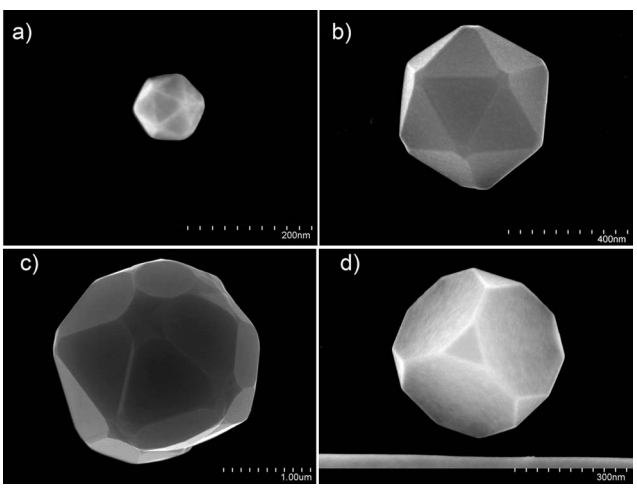

Fig. 11 Different icosahedral structures: (a) regular Au icosahedra, (b) Au icosahedra with some truncated corners, (c) heavily Au truncated icosahedra, and (d) Chui icosahedra.

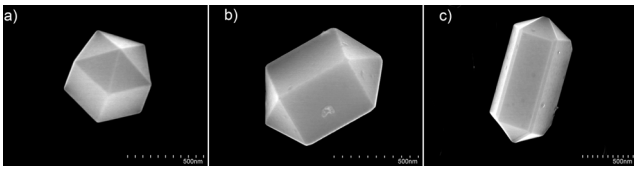

Fig. 12 Silver nanoparticles: (a) Ino type of decahedra, (b) larger Ino decahedra, and (c) nanowire which shows faceting on the edges.

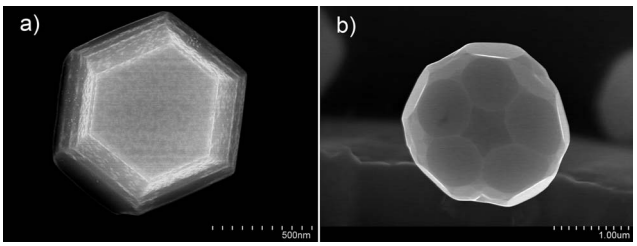

Fig. 13 (a) Larger Ag particle in which the growth is controlled by steps and (b) Au particle with the shape of a genus-41 Toroid.

observed. Fig. 11 shows examples of icosahedra with and without truncations. The icosahedrons truncated in the corners, producing (100) faces, have been described by Barnard[17] which explain the results of Chui *et al.*[18]

However it should be noticed that in some cases there is a growth of faces without truncation. This is the case shown in Fig. 12 that corresponds to the Ino decahedron[19] in which lateral facets grow until a nanorod is formed. However even in this case when the nanorod becomes larger truncations along the edges are observed.

It is very clear that in many cases the particles grow by step movement. That is very clear in Fig. 13 in which the steps are very clearly seen when particles are in the mesoscopic range. It is very clear that in many cases the particles grow by step movement, when the nanocrystals are in the mesoscopic range. Fig. 13a shows as an example of a typical particle growth by steps in this range. We can see remarkable shapes as the one in Fig. 13b, which corresponds to a genus-41 Toroid (also known as Webb toroid). We can see remarkable shapes such as the one in Fig. 13, which correspond to a genus-41 Toroid (also known as a Webb toroid), which is a remarkable structure.

Conclusions and discussions

By using Monte Carlo simulations in the grand canonical ensemble, we have been able to reproduce a number of morphologies obtained experimentally for both silver and gold nanoparticles. It is clear that faceting is required by a growing nanostructure. This is valid not only for decahedral or icosahedral faces but also even in the case of *fcc* structures. This is a remarkable finding in view of the previous work in which it was assumed that faceting will be only restricted to shapes which involve cyclic twinning such as the decahedra.

It is important to note that small changes in the activity of the ions produce significant changes in the chemical potential, which finally will result in a change on the nanoparticles morphology.

Our work also gives a very clear reason why shapes such as the decahedron and the icosahedrons, which are not observed in bulk crystals, can be seen in nanostructures from sizes of very few nanometres to sizes of micrometres.

Recently, there are some emerging approaches towards shape control of Au NPs involving the coherent utilization of surfactants.[20] However, despite the great success in the surfactant-assisted synthesis of shape-controlled NPs, some great challenges remain ahead in this research area, constituting an exciting topic for future work both experimentally and theoretically.

References

1 C. Herring, in *Structure and Properties of Solid Surfaces*, ed. R. G. Gomer and C. S. Smith, Chicago Press, 1953.
2 H. Ibach, *Physics of Surfaces and Interfaces*, Springer, New York, 2006.
3 M. C. Daniel and D. Astruc, *Chem. Rev.*, 2004, **104**, 293.
4 H. P. Bonzel, *Phys. Rep.*, 2003, **385**, 1.
5 B. Wiley, Y. Sun and Y. Xia, *Langmuir*, 2005, **21**(18), 8077.
6 S. Connor, F. Kim, H. Song, T. Kuykendall and P. Yang, *Angew. Chem., Int. Ed.*, 2004, **43**, 3673.
7 N. A. Oldani, M. M. Mariscal, S. A. Dassie and E. P. M. Leiva, *Faraday Discuss.*, 2008, **138**, 89.
8 L. Reinaudi, N. B. Luque, P. Serra and E. P. M. Leiva, *Electrochim. Acta*, 2009, **54**, 3011.
9 M. M. Mariscal, E. P. M. Leiva and O. A. Oviedo, *Phys. Chem. Chem. Phys.*, 2010, **12**, 10.
10 M. I. Baskes, S. M. Foile and M. S. Daw, *Phys. Rev. B: Condens. Matter Mater. Phys.*, 1986, **33**, 7983.
11 M. P. Allen and D. J. Tildesley, *Computer Simulations of Liquids*, Oxford University Press, 1989.
12 B. Wiley, T. Herricks, Y. Sun and Y. Xia, *Nano Lett.*, 2004, **4**(9), 1733.
13 L. D. Marks, *Surf. Sci.*, 1985, **150**, 358.
14 H. Hofmeister, *Cryst. Res. Technol.*, 1988, **33**, 3.
15 D. W. Deng and K. H. Kuo, *J. Alloys Compd.*, 2002, **342**, 174.
16 T. P. Martin, *Phys. Rep.*, 1996, **273**, 199.
17 A. Barnard, *Rep. Prog. Phys.*, 2010, **73**, 086502.
18 R. Ress, Y. H. Chui, I. Snook, B. O'Malley and S. P. Russo, *J. Chem. Phys.*, 2006, **125**, 114703.
19 S. Ino, *J. Phys. Soc. Jpn.*, 1969, **21**, 941.
20 J. Xiao and L. Qi, *Nanoscale*, 2011, **3**, 1383–1396.